



Pergamon

Available online at [www.sciencedirect.com](http://www.sciencedirect.com)

SCIENCE @ DIRECT®

Acta Materialia 51 (2003) 6415–6427



[www.actamat-journals.com](http://www.actamat-journals.com)

# Phase transformation kinetics and self-patterning in misfitting thin films

S.-B. Lee <sup>a</sup>, J.M. Rickman <sup>b,\*</sup>, K. Barmak <sup>a</sup>

<sup>a</sup> Department of Materials Science and Engineering, Carnegie Mellon University, Pittsburgh, PA 15213-3890, USA

<sup>b</sup> Department of Materials Science and Engineering, Lehigh University, 5 E. Packer Avenue, Bethlehem, PA 18015, USA

Received 3 May 2003; received in revised form 26 July 2003; accepted 14 August 2003

## Abstract

We outline a computational approach for the study of phase transformations in misfitting thin films and then investigate the kinetics of a transformation to assess the role of heterogeneous nucleation sites, formed in the vicinity of misfit dislocations, in the self-patterning of these systems. Both computer simulation and analytical methods are employed to analyze spatio-temporal correlations in the transforming phase as embodied, in particular, in the transformed volume fraction. To accomplish this, we first obtain an expression for the driving force for nucleation in terms of the strain energy stored in the film under site saturation conditions. This driving force forms the basis for simulations of nucleation and growth in films in which simulation parameters, such as film thickness and temperature, are systematically varied. We find that, in a fully coherent film, there is a retardation of the transformation at certain times that is associated with the constrained film geometry and that, in the presence of misfit dislocations, a range of kinetic behavior can be correlated with the relative magnitude of the driving forces and temperature. The implications of our results for pattern formation in these systems are then discussed.

© 2003 Published by Elsevier Ltd on behalf of Acta Materialia Inc.

*Keywords:* Nucleation of phase transformations; Simulation; Thin films

## 1. Introduction

Heteroepitaxial films composed of compound semiconductors, as well as various nitrides and oxides, are of significant technological and scientific interest given their use in numerous electronic, optoelectronic and photonic applications. For example, IV–IV heteroepitaxial structures of SiGe

and Si are employed in heterojunction bipolar transistors (HBT), while quantum wells and heteroepitaxial structures of III–V GaAs and related compounds find application in lasers and waveguides [1]<sup>1</sup>. The utility of these structures is perhaps best illustrated by the case of band-gap engineered HBTs, formed by the pseudomorphic growth of SiGe and Si layers to form the emitter–base–col-

\* Corresponding author. Tel.: +1-610-758-4236; fax: +1-610-758-4244.

E-mail address: [jmr6@lehigh.edu](mailto:jmr6@lehigh.edu) (J.M. Rickman).

<sup>1</sup> For a more extensive and detailed list of heterostructures and applications see Semiconductor Heterostructures for Photonic and Electronic Applications.

lector stack of the transistor. By careful control of the doping level in the emitter and collector regions and the Ge profile in the SiGe base region, and thus the associated band-gap narrowing in this region, bipolar transistors with record performance have been obtained [2].

Since the viability of the heterostructure devices noted above depends on the absence of threading and interfacial misfit dislocations, studies of heteroepitaxial film properties have focused, until recently, primarily on fully coherent layers [3–7]. Indeed, the presence of dislocations in certain device locations, such as the emitter–base–collector region of the Si–SiGe bipolar transistor, renders it non-functional, thus necessitating dislocation-free films. Given this need for fully coherently, heteroepitaxial films, substantial effort has been directed at the measurement and theoretical determination of critical film thicknesses below which there are no dislocations in mechanical equilibrium [5,6,8–10].

More recently, however, the interest in heterostructures has expanded to include not only semicoherent films [11,12], but also those films that undergo strain-driven morphological transitions to form organized arrays of islands or dots [13–18]. For example, the use of relaxed SiGe underlayers for growth of strained Si layers allows complementary metal-oxide-semiconductor (CMOS) field-effect transistors with faster switching speeds to be produced. Furthermore, strain-driven islanding leading to nanostructures that exhibit quantum confinement is highly relevant for optoelectronic devices. For semicoherent films there has been the additional realization that the spatially periodic elastic strains of the array of misfit dislocations can drive spinodal decomposition during film deposition and thus impart spatial periodicity to the decomposed film [19]. In short, misfit dislocations can lead to lateral self-patterning in heterostructures.

Given this possibility of tailoring patterned structures, it is of interest to examine the role of misfit dislocations in pattern formation for other types of phase transformations. Thus, in this paper, we outline a computational strategy for modeling nucleation and growth in misfitting thin films. Our aim is to use computer simulation and analytical

methods to assess the impact of an array of interfacial misfit dislocations on transformation kinetics. For simplicity and in order to obtain a quantitative understanding of the underlying kinetics, we consider an idealized model of a first-order transformation occurring in an elastically isotropic, misfitting film that is attached to a substrate. The transformation kinetics are quantified by calculating non-equilibrium correlation functions that embody nucleation and growth information (e.g., the volume fraction transformed, the one-point correlation function). From computer simulation we are able to determine how the system variables, including the driving forces, the temperature and the film dimensions, influence the transformation kinetics and associated microstructures. Having modeled a generic transformation, the relevance of our results to heteroepitaxial systems is then discussed.

This paper is organized as follows. In Section 2, the film and misfit geometries are discussed, the calculation of the stored elastic energy is summarized and the important contributions to the nucleation rate are highlighted. In Section 3, a description of the simulation methodology is presented. In Section 4, the simulation results for both a fully coherent film and one containing misfit dislocations are reviewed. Section 5 contains our conclusions and a discussion of points of technological and theoretical interest.

## 2. Misfitting film

Consider an elastically isotropic, misfitting thin film having thickness (height)  $h$  that is attached coherently to a substrate having the same elastic properties as the film. The lattice misfit parameter is denoted by  $f$ . For relatively large  $h$  the associated coherency strain energy is concomitantly large, and it can be favorable to nucleate misfit dislocations to relieve some of the strain energy stored in the film and substrate. Thus, in mechanical equilibrium, this system consists of a partially coherent film and periodic arrays of edge dislocations, each having Burgers vector  $\vec{b} = b\hat{x}$  and separated from one another by a distance  $d$ , at (or near) the film/substrate interface, as shown schematically in

Fig. 1. For simplicity, we consider here only a single misfit dislocation array.

Now suppose that the film undergoes a first-order phase transformation in response to a change in some parameter, such as the undercooling. The corresponding driving force for this transformation will depend not only on the undercooling, but also on the energy density associated with the remaining misfit strain, the strain field of the dislocation array and, in some cases, on the transformation strain. As our aim here is to describe quantitatively the kinetics of the nucleation and growth processes associated with a phase transformation in misfitting films we examine an idealized, yet tractable, model of this system wherein cylindrical nuclei, each having a critical radius, form *incoherently* in the film in a burst at time  $t = 0$  and subsequently grow (anisotropically) only in the radial direction. This model corresponds, then, to a two-dimensional slice of the transforming film with  $N$  nuclei appearing in a burst in the  $x$ - $y$  plane. One further simplification adopted here is that another possible eigenstrain, the transformation strain, is negligible. As will be seen below, these idealizations lead to a number of interesting and informative results, and other assumptions as to nucleation and growth rates and transformation strains can be readily incorporated into the model. Since the nucleation barrier, and therefore the nucleation rate, depend critically on the stored elastic energy, we first outline the calculation of the elastic fields associated with both a uniform misfit eigenstrain and with a periodic array of misfit dislocations.

## 2.1. Elastic fields

First, suppose that a fully coherent film with a misfit eigenstrain, confined to the film, is attached to a substrate. In the absence of dislocations the misfit parameter  $f$  plays the role of a coherency strain, and consequently the strain energy per unit film volume  $e_{\text{coh}} \propto f^2$  [4]. Following Tsao [4], upon introducing a single array of edge dislocations having a linear density  $\rho_{\pm} = 1/d$ , the effective coherency strain is reduced and the corresponding energy density is then

$$e_{\text{coh}} = \mu \left( \frac{1+\nu}{1-\nu} \right) [(f - \rho_{\pm} b)^2 + f^2], \quad (1)$$

where  $\mu$  and  $\nu$  are the shear modulus and Poisson ratio, respectively.

There is, of course, also an energy penalty associated with the introduction of a dislocation array by virtue of the attendant elastic distortion of the film and substrate. The elastic displacement and stress fields required to calculate this energy were obtained in Fourier space by Willis et al. [3] for a periodic array of dislocations in a homogeneous, elastically isotropic medium. The calculation of the corresponding real-space fields and the interpretation of the results in terms of image and corrective stresses are given in some detail in Appendix A. Given these stress field components  $\sigma_{ij}(\vec{r})$  at position  $\vec{r}$ , the dislocation energy density [20] is

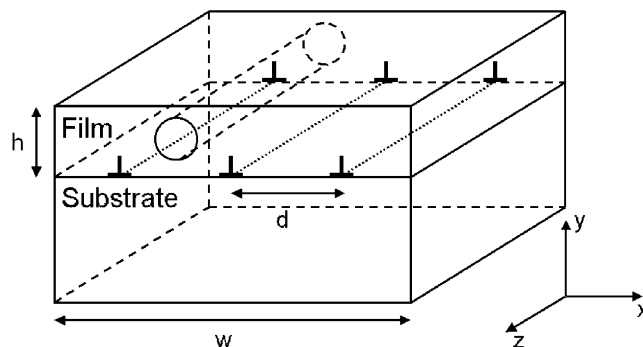


Fig. 1. A schematic of a misfitting thin film of height  $h$  attached to a substrate with equally-spaced misfit dislocations, separated by a distance  $d$ , at the film/substrate interface. Each dislocation has a Burgers vector  $\vec{b} = b\hat{x}$  and the system is periodically repeated in the  $x$ -direction. Also shown is a cylindrical critical nucleus (not to scale).

$$e_{\text{dis}}(\vec{r}) = \frac{1}{4\mu(1+\nu)}(\sigma_{11} + \sigma_{22} + \sigma_{33})^2 + \frac{1}{2\mu}(\sigma_{23}^2 + \sigma_{31}^2 + \sigma_{12}^2 - \sigma_{11}\sigma_{22} - \sigma_{11}\sigma_{33} - \sigma_{22}\sigma_{33}), \quad (2)$$

where the spatial indices 1, 2, and 3 correspond to  $x$ ,  $y$  and  $z$ , respectively.

Two remarks are in order here. First, we will, for simplicity, assume that the total energy density can be written as [8]  $e_{\text{coh}} + e_{\text{dis}}(\vec{r}) + e_{\text{core}}(\vec{r})$ , neglecting for the moment the issue of interactions between misfit and dislocation strain fields. (The core energy density  $e_{\text{core}}(\vec{r})$  is localized within a core radius about each dislocation.) It should be noted, however, that Willis et al. [3] have addressed the strain interaction issue and showed that, in some sense, it is possible to deconvolute different contributions to the total energy as has been done here. Furthermore, a similar, albeit approximate decomposition has been employed by other authors [4] to obtain tractable expressions for the misfit energy and the corresponding equilibrium misfit dislocation density, the latter being in good agreement with experiment. As we are interested in exploring a variety of nucleation scenarios, our discussion below focuses first on arbitrary misfit dislocation geometries before restricting consideration to those consistent with mechanical equilibrium. Second, it is important to note that because the misfit dislocation array (and its image) are not low-angle grain boundaries, some components of the dislocation stress field are necessarily long-ranged. In particular,  $\sigma_{11} = -2\mu b/d(1-\nu)$  as  $y \rightarrow \infty$ . Consequently, the catalytic effect of the misfit dislocations on the nucleation of a new phase is felt some distance from the film/substrate interface, at least for small  $d$  (i.e., relatively thick films).

## 2.2. Driving forces and nucleation rate

The nucleation rate of an incoherent, cylindrical solid phase having volume  $V$  and surface area  $A$  in an imperfect solid background can be deduced from the free energy change associated with the formation of a nucleus of the new phase. The

change in free energy  $\Delta G$  that attends heterogeneous, solid–solid nucleation is given by

$$\Delta G = -V\Delta G_v + A\gamma - \Delta G_{\text{def}}, \quad (3)$$

where  $\gamma$  is the solid–solid interfacial free energy (assumed to be isotropic),  $\Delta G_v$  is the driving “force” per unit volume for the transformation and  $\Delta G_{\text{def}}$  is the magnitude of the free energy released upon replacing a defected region with a nucleus of the new phase [21].

More specifically, for the system considered here [22,23],  $\Delta G_{\text{def}}$  has three major contributions: (1) the free energy associated with the removal of coherently strained material, namely  $(V-V_c)e_{\text{coh}}$ , where  $V_c$  is the core volume actually removed; (2) the free energy associated with the removal of the dislocation core volume, namely  $V_c e_{\text{core}}$  (where  $e_{\text{core}}$  is constant within the volume  $V_c$ ); and (3) the free energy associated with the removal of film volume that is deformed due to the elastic fields

of the dislocation array, namely  $\int_{V-V_c} d^3r e_{\text{dis}}(\vec{r})$ .<sup>2</sup>

This latter expression depends implicitly on the location of the center of the nucleus,  $\vec{r}_0$ .

Having determined the various contributions to the formation free energy, the energy barrier per unit length to create a critical nucleus is obtained by first maximizing  $\Delta G$  with respect to the radius of the nucleus and then calculating  $\Delta G$  at that radius, hereafter denoted as  $\Delta G^*$ . For simplicity, the length  $l$  of the cylindrical nucleus is fixed here to obtain a two-dimensional model. (The shape of a critical nucleus in three dimensions for systems containing dislocations has been considered elsewhere [22].) Although this calculation can be done directly using Eq. (3), it will be convenient in our lattice simulations (see below) to focus on nuclei that form on a dislocation line and remove only dislocation core volume (i.e.,  $V=V_c$ ) and those that form off a dislocation line and remove no core volume (i.e.,  $V_c=0$ ). In the former case the associated free energy barrier is taken to be  $\Delta G_{\text{core}}^*$  while, in the latter case, one finds that

<sup>2</sup> The limit  $V-V_c$  denotes an integration over the volume of the nucleus not overlapping with a dislocation core.

$$\Delta G^*(\vec{r}_0) = \frac{\pi\gamma^2}{(\Delta G_v + e_{\text{coh}} + e_{\text{dis}}(\vec{r}_0))}, \quad (4)$$

where, to obtain a tractable expression, it is assumed that a nucleus is sufficiently small so that

$$\int_V d^3r e_{\text{dis}}(\vec{r}) \approx (V)e_{\text{dis}}(\vec{r}_0) \quad (5)$$

The nucleation rate per unit area in the  $x$ - $y$  plane,  $I(\vec{r}, t)$ , for a burst of embryos forming at temperature  $T$  can then be determined from the free energy barrier from

$$I(\vec{r}, t) = n(\vec{r})\delta(t), \quad (6)$$

where  $n(\vec{r}) = n_0 \exp(-\Delta G^*(\vec{r})/k_B T)$  is the number of nuclei per unit area at time  $t = 0$  and  $k_B$  is Boltzmann's constant. For simplicity, it is assumed that the prefactor  $n_0$ , which reflects the number of potential nucleation sites per unit area, is constant throughout the film. The total number of nuclei in a slice of the system just after the burst is then  $N = \int d^2r n(\vec{r})$ , where the integration is performed over the  $x$ - $y$  plane.

### 3. Transformation simulation

Given the complexity of nucleation and growth scenarios in a misfitting thin film, it is useful to simulate these processes to gain a better understanding of the interplay among various geometrical and kinetic factors. Towards this end, we performed simulations of a first-order phase transformation incorporating the simplifying assumptions outlined in the previous section. To highlight the impact of catalytic sites on the nucleation stage of the transformation, we do not consider here modifications of the growth rate of the new phase. (Such modifications may be of importance in some systems, and will be the subject of a future investigation.) In particular, we used the Monte Carlo (MC) method [24] to determine the distribution of critical nuclei, followed by a Voronoi-generating growth simulation [25,26] of the resulting transformation. Our motivation for selecting the MC method to determine the position of the nuclei was that, since the probability density

$p(\vec{r})$  of critical nuclei at fixed temperature and other parameters is given by

$$p(\vec{r}) = \frac{n(\vec{r})}{N} \propto \exp(-\Delta G^*(\vec{r})\ell/k_B T), \quad (7)$$

the spatial distribution of critical nuclei could be generated via the Metropolis method [27] in a manner similar to that used to generate an equilibrium configuration for a collection of interacting particles in the canonical ensemble. That is, we first randomly distribute the  $N$  "nuclei" in the region of interest and treat them as a lattice gas that can be equilibrated by a series of single-particle displacements, subject to the constraint of single site occupancy and consistent with the requirements of detailed balance. The MC procedure then guarantees that the configurations will eventually be those characteristic of thermodynamic equilibrium. In this case, the resulting configurations will be those consistent with the distribution of critical nuclei drawn from  $p(\vec{r})$ .<sup>3</sup>

From Eq. (4), it is clear that the transformation kinetics are determined by the relative magnitudes of several physical quantities. By choosing  $b$  and  $\mu b^3$  as the fundamental length and energy units, respectively, one can identify the following dimensionless variables as the input simulation parameters:  $\bar{\gamma} = \gamma/\mu b$ ,  $\Delta\bar{G}_v = \Delta G_v/\mu$ ,  $\bar{e}_{\text{coh}} = e_{\text{coh}}/\mu$ ,  $\bar{e}_{\text{dis}}(\vec{r}_0) = e_{\text{dis}}(\vec{r}_0)/\mu$  and  $\bar{T} = k_B T/(\mu b^3)$ . For convenience, we take  $\ell = b$  and  $\nu = 0.25$ . Selected regions in this multidimensional parameter space will be probed in the simulation results presented in the next section.

The details of our implementation are as follows. For a given set of physical parameters the probability density  $p(\vec{r})$  is determined. As the growth of the product phase is assumed to be negligible in the  $z$ -direction, we employ a square lattice in the  $x$ - $y$  plane, with lattice parameter  $b$  that is periodic in two dimensions, containing a strip with

<sup>3</sup> In this context the implementation of the Metropolis method involves calculating the change in  $\Delta G^*$  upon attempting to move a nucleus. If this move lowers the formation energy, it is accepted whereas, if the formation energy increases, it is accepted with a probability that depends exponentially on the change in  $\Delta G^*$ . Consequently, nuclei move preferentially to regions of high strain energy density.

dimensions  $w \times h$  that represents the film. The film width  $w$  is chosen as an integral multiple of the dislocation spacing  $d$ , consistent with a misfit dislocation array. These lattice sites comprise the set of nucleation locations  $\{\vec{r}_0\}$ . This spatial discretization and assignment of nuclei is reasonable here for a number of systems of interest. For example, in polymorphic transformations in FePt and CoPt systems with chemical driving forces in the range of 1–10 kJ/mole [28] and interfacial free energy of about 400 mJ/m<sup>2</sup> (consistent with the assumption of an incoherent interface) the critical radius is in the range of about 4–10 Å (or about  $2b$ ). Although one should, in principle, adjust the size of the lattice parameter with changes in driving force, etc., to reflect corresponding changes in critical radius, we shall not do so in this paper.

After the MC equilibration that determines the distribution of the  $N$  critical nuclei from  $p(\vec{r})$ , these nuclei grow at a constant radial growth rate to impingement so as to mimic interface-controlled kinetics. Other nucleation and growth rate assumptions are, of course, readily implemented as well. The limitations imposed by the film boundaries are enforced by considering only the area transformed and the attendant microstructures in the strip itself while allowing the growth of the product phase to consume the entire lattice. The calculation of non-equilibrium correlation functions, such as those related to the area fraction transformed, are performed after repeating the transformation simulations many times for different realizations of the initial conditions. Finally, we note that for a nucleation scenario that differs from this one in one or more of the simulation parameters, the number of nuclei,  $N'$ , in the current scenario is given by

$$N' = N \frac{\int d^2r \exp(-\Delta G'^*(\vec{r})\ell/k_B T)}{\int d^2r \exp(-\Delta G^*(\vec{r})\ell/k_B T)}, \quad (8)$$

where the integration is performed over the film area in the  $x$ - $y$  plane.

For reference, we summarize here the main assumptions employed in the transformation simulations.

1. A fixed number of nuclei appear in a burst (i.e., site saturation conditions) and subsequently grow at a constant radial rate until impingement.
2. The presence of dislocations alters the spatial distribution, though not the total number, of nuclei.
3. A critical nucleus is taken to be cylindrical in shape.
4. In cases, where misfit dislocations are present, the dislocation core energies are ignored in order to focus on the energetics associated with long-ranged strain fields.
5. The growth rate of the new phase is unaffected by the presence of the dislocations.

## 4. Simulation results and interpretation

### 4.1. Fully coherent film

Before examining the kinetics and microstructures associated with phase transformations in the presence of misfit dislocations, it is useful to quantify the transformation kinetics in a fully coherent, misfitting film. While the spatio-temporal correlations of a transforming phase in infinite, periodic and defected systems have been discussed elsewhere [26,29–31], it is worth noting that the confined geometry of the film here leads to observable differences with bulk systems. Thus, the fully coherent, misfitting film system is an important baseline for comparing other defected systems examined here.

For concreteness, we consider the time-dependence of the one-point correlation function associated with the area fraction transformed in a misfitting film under site-saturation conditions in which the nuclei are randomly distributed throughout the film with areal density  $n(\vec{r}) = n \Theta(y) \Theta(h-y)$ , where  $\Theta$  is the step function. There are three relevant length scales for this system, and it is convenient then to introduce dimensionless time and height variables,  $\bar{t} = \sqrt{nGt}$  and  $\bar{h} = \sqrt{nh}$ , respectively. Fig. 2 shows the (average) area fraction transformed,  $\phi(\bar{t})$ , for two different film geometries that differ in the reduced film height,  $\bar{h}$ , while the corresponding microstructures are given in Fig. 3. The results displayed in Fig. 2

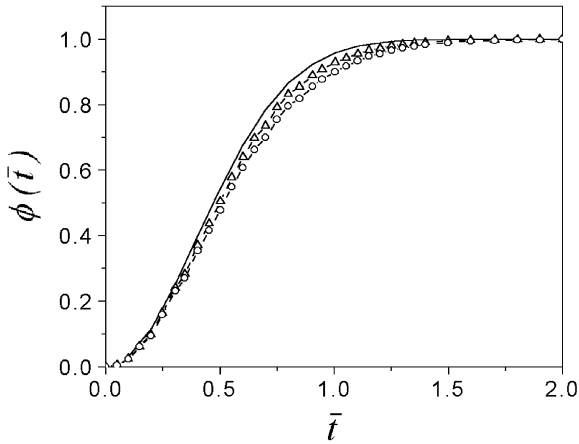


Fig. 2. The area fraction transformed,  $\phi(\bar{t})$ , as a function of reduced time,  $\bar{t}$ , for an infinite system (upper line) and for two finite-sized films having  $\bar{h} = 1.8$  ( $\times$ ) and  $\bar{h} = 3.5$  ( $\Delta$ ), respectively. The simulation results were average over  $10^4$  starting configurations. The solid and dashed lines were determined analytically using Eqs. (11) and (12). Note that the agreement between the simulation and analytical results is excellent.

represent averages over  $10^4$  independent runs for each geometry. As is evident from the figure, the sharp terminations of the transformation at the film/substrate and film/vacuum interfaces increase the transformation completion time as  $\bar{h}$  decreases.

An analytical representation of the data in Fig. 2 follows from earlier work by Sekimoto [29] and can be deduced from stochastic geometric considerations as follows. If the randomly distributed nuclei subsequently grow at constant radial growth rate  $G$ , then the probability that at least one nucleus transforms a point with coordinates  $(x, y)$ , ( $0 \leq y \leq h$ ) at time  $t$  is found from the Poisson distribution to be  $P(x, y) = 1 - \exp(-\Lambda(x, y))$ , where  $\Lambda(x, y)$  is the expected number of nuclei at a distance less than  $Gt$  from  $(x, y)$ . Thus,  $\Lambda(x, y)$  can be written in

terms of that area of a circle of radius  $Gt$  lying within the film as

$$\Lambda = n\pi G^2 t^2 [1 - f(y/Gt) - f((h-y)/Gt)], \quad (9)$$

$$(0 \leq y \leq h)$$

where

$$f(s) = \frac{1}{\pi} \left[ \cos^{-1}(s) - \sqrt{1-s^2} s \right] \Theta(1-s). \quad (10)$$

Finally,  $\phi(\bar{t})$  can be calculated from  $P(x, y)$  by an integration over the film area that, given that  $\Lambda$  is independent of  $x$ , yields

$$\phi(\bar{t}) = 1 - \exp(-\pi \bar{t}^2) \psi(\bar{h}, \bar{t}), \quad (11)$$

where the film geometry function

$$\psi(\bar{h}, \bar{t}) = \frac{1}{\bar{h}} \int_0^{\bar{h}} d\bar{y} \exp(\pi \bar{t}^2 f(\bar{y}/\bar{t})) \exp(\pi \bar{t}^2 f((\bar{h}-\bar{y})/\bar{t})). \quad (12)$$

In the limit  $\bar{h} \rightarrow \infty$  one finds that  $\psi \rightarrow 1$  as expected. Also shown in Fig. 2, are  $\phi(\bar{t})$ , as calculated by numerical integration from Eq. (12), for the two film geometries considered above. Clearly there is excellent agreement between the simulation and analytical results.

The behavior exhibited in Fig. 2, can also be understood somewhat more intuitively. At early times ( $\bar{t}/\bar{h} < 1$ ) relatively few transforming domains are impeded by the film/substrate and film/vacuum boundaries and, hence,  $\phi(\bar{t}) \approx 1 - \exp(-\pi \bar{t}^2)$  in this regime. At intermediate times ( $\bar{t}/\bar{h} > 0.5$ ) the region about any point in the film available for transforming this point at time  $t$  decreases, and so the corresponding number of nuclei available for this purpose also decreases. This decrease in the number of transforming nuclei



Fig. 3. The microstructures corresponding to nucleation in films having (a)  $\bar{h} = 1.8$  and (b)  $\bar{h} = 3.5$ , respectively. The boundary conditions alter the distribution of grain areas relative to that of an infinite system.

tends to increase the time required to transform a given region, thereby slowing the transformation relative to that in an infinite system. At late times the transformation approaches completion and consequently  $\phi(\bar{t}) \rightarrow 1$ . The retardation of the transformation associated with thin films can also be illustrated by considering the extreme case of  $\bar{h} < \ll 1$ . In this limit the system is quasi-one-dimensional, with  $\phi(\bar{t}) \approx 1 - \exp(-\bar{h}\bar{t})$ , and the transformation half-life  $\bar{t}_{1/2} = \ln(2)/\bar{h}$ . This half-life is larger than that for an infinite two-dimensional system if  $\bar{h} < 2.62$ .

#### 4.2. Misfitting film with dislocations

If it is energetically favorable to have misfit dislocations at the film/substrate interface, these defects may catalyze the nucleation of a new phase that forms in the film. The relative potency of these catalytic sites determines the spatial distribution of nucleation sites and can therefore be inferred from the time-dependence of the one-point function. This relationship between the one-point function and the nucleation conditions is illustrated below by considering prototypical nucleation scenarios and then developing an analytical approximation to the one-point function.

In each scenario the spatial distribution of  $N = 100$  nuclei in a system containing five equally spaced edge dislocations is determined from Eq. (7). Several cases are examined here, each corresponding to a different reduced temperature in the range of  $0.002 \leq \bar{T} \leq 0.02$ , with the following simulation parameters:  $\bar{\gamma} = 0.1$  and  $\Delta\bar{G}_v = 0.04$ .<sup>4</sup> As indicated above, the core energy was taken to be zero here to highlight the effect of other catalytic sites. Clearly, there are many situations in which the energy of the core region is relatively high, leading to preferential nucleation on the core. In any case,

non-zero core energies are also readily included in this model.

The one-point functions for these cases are presented in Fig. 4 and illustrative, low-temperature microstructures are given in Fig. 5. At low-temperature, as is evident from Fig. 5, the nuclei “decorate” the high strain energy dislocation regions while, at higher temperatures, sites further from the dislocations having somewhat higher nucleation barriers are sampled as well. We note that the single-occupancy site constraint on the nuclei sometimes traps the system into metastable states, and so relatively long MC runs (over  $10^5$  steps per nucleus) are employed here to determine the equilibrium distribution of nucleation sites.

Two remarks concerning Fig. 4 are in order. First, as compared with the transformations in fully coherent films (see Fig. 2),  $\phi(\bar{t})$  does not have a sigmoidal shape at low-temperature, and the associated completion time for the transformation is shifted to late times. Second, at higher temperatures, the one-point function more closely resembles those seen in fully coherent films. This result is expected since the catalytic effect of the

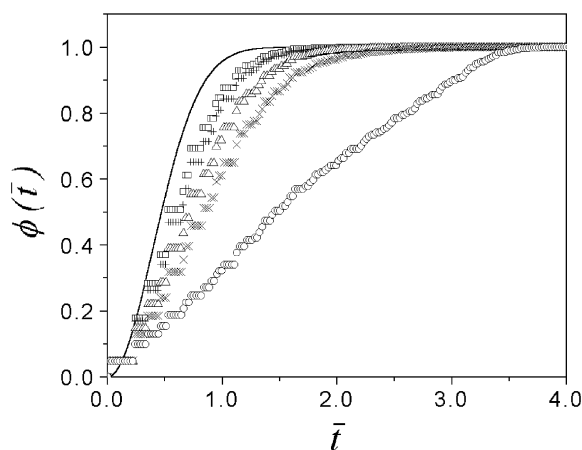


Fig. 4. The area fraction transformed,  $\phi(\bar{t})$ , as a function of reduced time,  $\bar{t}$ , for a film with  $h = 20b$  and  $w = 100b$  having five misfit dislocations. The results for several different reduced temperatures,  $\bar{T} = 0.002$  ( $\circ$ ),  $0.0075$  ( $\times$ ),  $0.01$  ( $\triangle$ ),  $0.015$  ( $+$ ) and  $0.02$  ( $\square$ ), are presented along with the curve for an infinite system. As  $\bar{h} \approx 4.5$ , the film-size correction is small and therefore not considered here. (See Fig. 2.) The jaggedness of the curves at early reduced times is an artifact of spatial discretization in the simulation.

<sup>4</sup> The fact that the total number of nuclei is 100 here means that the prefactor  $n_0$  (see Eq. (6)) has been determined. Also, upon changing the temperature one should, in principle, adjust the chemical driving force and the total number of nuclei in the simulation cell, the latter according to Eq. (8). This is not done here in order to simplify the comparison of the transformation kinetics.

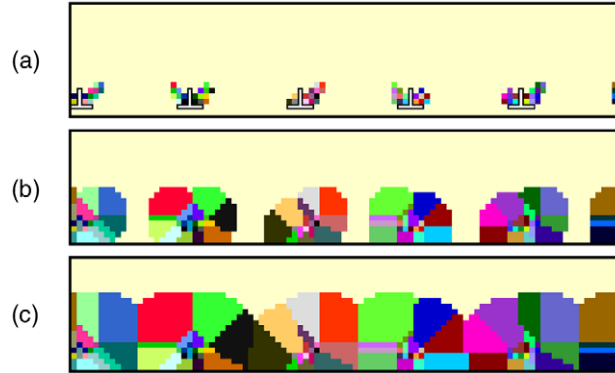


Fig. 5. The microstructures corresponding to nucleation in a  $20b \times 100b$  film for  $\bar{T} = 0.002$  at  $\bar{t} = 0.22, 1.12$  and  $2.91$ , respectively. The misfit dislocations have also been sketched in (a). Note that the system evolves approximately as a series of corrugated blocks. The distribution of nuclei about a given dislocation can be rationalized by noting that, for an isolated edge dislocation,  $e_{\text{dis}} = (1/2\mu) \left( \frac{\mu b}{2\pi(1-\nu)r} \right)^2 (1-2\nu \sin^2(\phi))$ , where  $\phi$  is an azimuthal angle measured from the  $+x$ -axis. In this low-temperature example, nucleation takes place preferentially in regions of high  $e_{\text{dis}}$ .

dislocations is, to some degree, mitigated by higher temperatures. In fact, at the highest temperatures considered here, the fully coalesced microstructures are similar to those given in Fig. 3.

As before, an analytical representation of the transformation curves follows from the theory of point processes [32] and geometrical considerations. Consider first the low-temperature transformation kinetics associated with nuclei clustered around individual dislocations. For simplicity, we neglect for the moment the spatial extent of the nucleation “clouds” and imagine that an oversized particle containing  $M$  nuclei is located at each dislocation core, where  $M \gg 1$  is the number of nuclei per dislocation. The corresponding nucleation is then  $n(\vec{r}) = M \sum_i \delta(x-di) \delta(y)$ , where the sum is over all dislocations (separated by  $d$ ) in the system. Following the same procedure as outlined above, the area fraction transformed can be deduced from the probability that at least one oversized particle transforms a given point such that, for  $d < 2h$ ,

$$\phi \approx 1 - \left( \frac{1}{hd} \right) \int_{-d/2}^{d/2} \int_0^h dx dy \exp[-M\Theta(G^2t^2 - x^2 - y^2)] = \left( \frac{1}{hd} \right) (1 - e^{-M}) \pi G^2 t^2 g(d/2Gt, h/Gt), \tag{13}$$

where the film geometry function

$$g(s, w) = \frac{1}{2} \Theta(s-1) + \frac{1}{\pi} \left( \sin^{-1}(s) + \sqrt{1-s^2} s \right) \Theta(1-s) \Theta(w^2 + s^2 - 1) - f(w) \Theta(1-w) \Theta(w^2 + s^2 - 1). \tag{14}$$

Thus, for  $Gt \gg d/2$ , one finds that  $\phi(t) \propto Gt$ , as seen in Fig. 4 over a wide range of time. Furthermore, for  $Gt = h$ , a Taylor series expansion of Eq. (14) yields  $\phi \approx 1 - (1/24)(d/h)^2$  and so the nonlinear termination of the transformation curves are due to the corrugated nature of the transforming interface.<sup>5</sup> We note, however, that the quadratic dependence of  $\phi(t)$  on time predicted by Eq. (13) for early times does not capture well the corresponding behavior in the figure. This disparity is due to the idealization of the nucleation density inherent in this simplified description. As is evi-

<sup>5</sup> In Eq. (14) we consider a transformation cell associated with a single dislocation. Thus, the first term is associated with the area of a semicircle prior to impingement on the side walls of the cell. The second term is associated with the area after side-wall impingement until the end of the transformation. The third-term is a correction to that area due to the truncation associated with the film height.

dent from Fig. 5, a spatially extended distribution of nuclei leads to a series of evolving, corrugated blocks whose moving fronts, even at relatively early times, result in a nearly linear dependence of  $\phi(t)$  on time.

A tractable, analytical representation of the high-temperature transformation curve is more difficult to construct owing to the complex distribution of nucleation sites. Nevertheless, an approximation to  $\phi(t)$  follows from the somewhat arbitrary division of nucleation sites into two broad classes, those near the dislocations ( $Mw/d$ ) and those farther away at bulk sites. If it is assumed that the bulk nuclei are essentially randomly distributed with a density  $n_b$ , then the total density, neglecting the cutoff near the dislocations, is approximately

$$n(\vec{r}) \approx M \sum_i \delta(x-di)\delta(y) + n_b \Theta(y) \Theta(h-y), \quad (15)$$

where, again  $N = \int d^2r n(\vec{r})$ . Having determined  $M$  from the distribution of nuclei, then

$$\phi(t) = 1 - \frac{1}{hd} \int_{-w/2}^{w/2} \int_0^h dx dy \exp \left[ - \int \int_0^h dx' dy' n(x', y') \Theta(G^2 t^2 - (x-x')^2 - (y-y')^2) \right]. \quad (16)$$

While it is possible to evaluate Eq. (16) numerically, we present here only our simulation results. The impact of temperature on transformation kinetics is illustrated in Fig. 6 wherein the reduced half-life for a transformation is given as a function of reduced temperature. As is evident from the figure, the half-life decreases with increasing temperature, a result that follows from the fact that, upon decreasing  $M$ , the kinetics of the system more closely resembles that of spatially random nucleation and subsequent growth.

## 5. Conclusions

We have outlined here a computational approach for the study of phase transformations in thin films

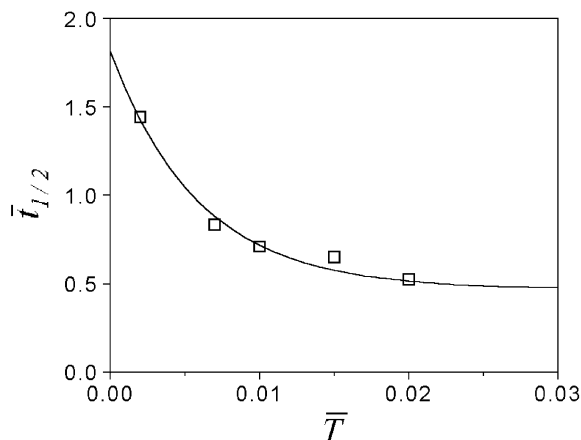


Fig. 6. The reduced half-life of a transformation (i.e., the reduced time elapsed for 50 transformation)  $\bar{t}_{1/2}$ , vs. reduced temperature,  $\bar{T}$ , for a series of transformations in a misfitting film. The temperature controls the fraction of nuclei near the dislocations. Thus, as  $\bar{T}$  increases, the half-life approaches that associated with spatially random nucleation. The solid line represents a fit to the simulation data given by  $\bar{t}_{1/2} = 0.47 + 1.34 \exp(-169.83\bar{T})$ . For comparison, we note that the half-life for spatially random nucleation in an infinite system is  $\bar{t}_{1/2} = \sqrt{\ln(2)/\pi} = 0.47$ .

and assessed the catalytic role of misfit dislocations in transformation kinetics in self-patterning systems. This was accomplished by the calculation of the time-dependence of the transformed volume fraction via computer simulation and analytical methods. We find that, in a fully coherent film, there is a retardation of the transformation at intermediate times as the film thickness decreases. Furthermore, in the presence of misfit dislocations, a range of kinetic behavior is observed and correlated with the relative magnitude of the driving forces and the temperature. More generally, our results allow one to relate the functional form of the transformation curve to the spatial distribution of catalytic sites.

This work raises several issues of both technological and theoretical relevance. First, it is of interest to determine whether the transformation kinetics and associated microstructures can be controlled experimentally. From the foregoing discussion it is clear that the morphology of the transforming microstructure results from a complicated interplay among geometric variables and driving

forces. In particular, the film height determines the equilibrium dislocation spacing and therefore the spatial distribution of catalytic sites. To see this most directly, one constructs the areal energy density (in the  $x$ - $z$  plane) in the film and, by minimizing this areal density with respect to  $\rho_{\perp}$ , determines the dependence of the equilibrium dislocation spacing,  $d = 1/\rho_{\perp,eq}$ , on  $h$ . As this calculation is straightforward, but rather tedious using Eqs. (1) and (2), we merely note that for widely separated dislocations  $\rho_{\perp,eq}$  increases with increasing film height, provided that  $h$  is greater than the critical film thickness.

From these energetic considerations it is evident that, as  $h$  increases above  $h_c$ , the equilibrium dislocation spacing decreases, and so cells in the transformed microstructure can have a lateral spacing commensurate with  $d$  under conditions, for example, of large dislocation site potency (e.g.,  $\bar{e}_{dis}/\bar{e}_{coh} \gg 1$  near dislocations). Furthermore, if the core energies are relatively large, a columnar microstructure is also expected. The dominant role of near dislocation and core sites in determining microstructure and kinetics is mitigated, to some extent, by the fact that some components of the stress field due to the dislocations are long-ranged, thereby making nominal bulk sites somewhat more attractive for nucleation. We also note that at sufficiently large  $h$  (small  $d$ ) dislocation–dislocation interactions become increasingly important, with the result that  $e_{dis}$  exhibits local minima between the dislocations and, hence, the potency of these intermediate sites is reduced. In short, the film thickness determines the spatial distribution of site potencies, while site occupancies are governed largely by the relative magnitude of chemical and strain energy driving forces, as well as the absolute temperature. A detailed study of the impact of film height, and therefore equilibrium dislocation spacing, on transformation microstructure is the subject of future work.

With regard to the heteroepitaxial systems discussed in the Introduction, the methods outlined in this work permit the quantitative, parametric design of films with prescribed transformation paths and patterned microstructures. Furthermore, the results presented here, and in the previous section, allow one to construct kinetic and microstruc-

tural maps that link some measures of transformation time and grain morphology with the set of geometric, mechanical and thermodynamic variables (e.g., Figs. 5 and 6).

Another issue following from this work concerns a class of transformations, not considered here, in which the new phase forms coherently in a crystalline background. In this case, the deformation of the elastically anisotropic background that attends nucleation induces spatial correlations among the nuclei since there are now “hard” and “soft” crystallographic directions. A proper treatment of these correlations will necessitate some modifications of the foregoing development along the lines of earlier investigations that exploited the formalism of the statistics of non-random point processes. [33,34] These modifications are also the subject of ongoing work.

## Acknowledgements

The authors acknowledge the final support of the MRSEC program of the National Science Foundation under DMR-0079996, Seagate Technology and the PTIA program of the Commonwealth of Pennsylvania. The authors also thank Dr. J. Kim for his assistance in preparing the manuscript.

## Appendix A

On physical grounds, the stress field components  $\sigma_{ij}(x,y)$  in the film due to the misfit dislocations can be regarded as the superposition of the fields due to (1) the array of misfit dislocations itself, (2) an image array (with each dislocation having  $\vec{b} = -b\hat{x}$ ) located a distance  $h$  above the film/vacuum interface and (3) any corrective forces needed to ensure that the net tractions on the film/vacuum interface are zero.

The dislocation stresses may be deduced by examining the stresses associated with a single edge dislocation, having  $\vec{b} = b\hat{x}$  and line direction  $\hat{l} = \hat{z}$ , located in an infinite, elastically isotropic medium with shear modulus,  $\mu$ , and Poisson ratio  $\nu$ . The non-zero stress components for this isolated dislocation are given by [20,35]

$$\begin{aligned} \sigma_{11}^+(x,y) &= -\frac{\mu b}{2\pi(1-\nu)} \frac{y(3x^2 + y^2)}{(x^2 + y^2)^2}, \\ \sigma_{22}^+(x,y) &= \frac{\mu b}{2\pi(1-\nu)} \frac{y(x^2 - y^2)}{(x^2 + y^2)^2}, \\ \sigma_{12}^+(x,y) &= \frac{\mu b}{2\pi(1-\nu)} \frac{x(x^2 - y^2)}{(x^2 + y^2)^2}, \\ \sigma_{33}^+(x,y) &= \nu(\sigma_{11} + \sigma_{22}), \end{aligned} \tag{A.1}$$

The boundary conditions at the film vacuum interface required that  $\sigma_{i,2}(x,h) = 0$  for  $i = 1,2,3$ . Now, since a trial solution of the form  $\sigma_{ij}^+(x,y) - \sigma_{ij}^+(x,y-2h)$  does not vanish at  $y = h$  for  $i = j = 2$ , it is necessary to add to this combination corrective stresses that yield  $-2\sigma_{22}^+(x,h)$  while maintaining  $\sigma_{1,2}(x,h) = \sigma_{3,2}(x,h) = 0$ . The appropriate corrective stress can be obtained by integrating the needed tractions against the Green tensor for an isotropic half space [36].

Several authors have examined the elasticity problem for a misfitting thin film [3,37]. In particular, the stress field for the dislocation array shown in Fig. 1 has been obtained by Willis et al. [3] in a reciprocal space formulation. To compare this solution with the analysis in terms of images outlined above, it is useful to obtain the corresponding stress components in real-space. Upon inverting the one-dimensional Fourier transform for a single dislocation and then summing the resulting stresses over an infinite dislocation array (with dislocation separation  $d$ ) one finds that

$$\sigma_{ij}(x,y) = \sum_{n=-\infty}^{n=+\infty} [\sigma_{ij}^+(x + nd,y) - \sigma_{ij}^+(x + nd,y-2h)] \tag{A.2}$$

$$(x + nd,y-2h) + \sigma_{ij}^{\text{corr}}(x + nd,y)],$$

where the non-zero corrective stresses are given by

$$\sigma_{11}^{\text{corr}}(x,y) = -2h \frac{(y-2h)^2 - x^2}{((y-2h)^2 + x^2)^2} \tag{A.3}$$

$$+ 4h (y-2h)(y-h) \frac{(y-2h)^2 - 3x^2}{((y-2h)^2 + x^2)^3},$$

$$\sigma_{22}^{\text{corr}}(x,y) = 2h \frac{(y-2h)^2 - x^2}{((y-2h)^2 + x^2)^2} \tag{A.4}$$

$$+ 4h (y-2h)(y-h) \frac{(y-2h)^2 - 3x^2}{((y-2h)^2 + x^2)^3},$$

$$\sigma_{12}^{\text{corr}}(x,y) = 4hx (y-h) \frac{3(y-2h)^2 - x^2}{((y-2h)^2 + x^2)^3} \tag{A.5}$$

These solutions can also be obtained via the calculation of the Airy stress function for a dislocation near a phase boundary[19,38].

The summations for some of the terms in the above equations have already been performed elsewhere [20]. For example, one finds that

$$\begin{aligned} \sum_{n=-\infty}^{n=+\infty} \frac{y^2 - (x + nd)^2}{[(x + nd)^2 + y^2]^2} \\ = \frac{2\pi^2}{d^2} f_1(x,y)f(x,y), \end{aligned} \tag{A.6}$$

$$\begin{aligned} \sum_{n=-\infty}^{n=+\infty} y \frac{3(x + nd)^2 + y^2}{[(x + nd)^2 + y^2]^2} \\ = \left(\frac{\pi}{d}\right) \left[ 2\sinh\left(\frac{2\pi y}{d}\right) f_2(x,y) \right. \\ \left. - 2\pi\left(\frac{y}{d}\right) f_1(x,y) \right] f(x,y), \end{aligned} \tag{A.7}$$

$$\begin{aligned} \sum_{n=-\infty}^{n=+\infty} \frac{(x + nd) [(x + nd)^2 - y^2]}{[(x + nd)^2 + y^2]^2} \\ = \left(\frac{\pi}{d}\right) \sin\left(\frac{2\pi x}{d}\right) \end{aligned} \tag{A.8}$$

$$\left[ f_2(x,y) - 2\pi\left(\frac{y}{d}\right) \sinh\left(\frac{2\pi y}{d}\right) \right] f(x,y),$$

where

$$f_1(x,y) = \left[ \cosh\left(\frac{2\pi y}{d}\right) \cos\left(\frac{2\pi x}{d}\right) - 1 \right], \tag{A.9}$$

$$f_2(x,y) = \left[ \cosh\left(\frac{2\pi y}{d}\right) - \cos\left(\frac{2\pi x}{d}\right) \right], \tag{A.10}$$

$$f(x,y) = \left[ \cosh\left(\frac{2\pi y}{d}\right) - \cos\left(\frac{2\pi x}{d}\right) \right]^{-2} \tag{A.11}$$

The remaining summations can be performed by using Eq. (A.6) as a generating function since

$$\frac{\partial}{\partial y} \left[ \sum_{n=-\infty}^{n=+\infty} \frac{(x + nd)^2 - y^2}{[(x + nd)^2 + y^2]^2} \right] = \tag{A.12}$$

$$\begin{aligned}
 & -2y \left[ \sum_{n=-\infty}^{+\infty} \frac{3(x+nd)^2 - y^2}{[(x+nd)^2 + y^2]^3} \right], \\
 & \frac{\partial}{\partial x} \left[ \sum_{n=-\infty}^{+\infty} \frac{(x+nd)^2 - y^2}{[(x+nd)^2 + y^2]^2} \right] \\
 & = -2 \left[ \sum_{n=-\infty}^{+\infty} (x+nd) \frac{(x+nd)^2 - 3y^2}{[(x+nd)^2 + y^2]^3} \right]
 \end{aligned} \tag{A.13}$$

## References

- [1] Tu CW, Houghton DC, Tung RT, editors. *Mater Res Sci Proc* 1993;281.
- [2] Meyerson BS. *Appl Phys Lett* 1986;48:797.
- [3] Willis JR, Jain SC, Bullough R. *Phil Mag* 1990;A62:115.
- [4] Tsao JY. *Materials fundamentals of molecular beam epitaxy*. New York: Academic Press Inc, 1993.
- [5] Mathews JW, Blakeslee AE. *J Cryst Growth* 1974;27:118.
- [6] Mathews JW, Blakeslee AE. *J Cryst Growth* 1975;29:273.
- [7] Osbourn GC. *J Appl Phys* 1982;53:1586.
- [8] Frank FC, van der Merwe J. *Proc R Soc* 1949;A198:216.
- [9] People R, Bean JC. *Appl Phys Lett* 1985;47:322.
- [10] People R, Bean JC. *Appl Phys Lett* 1986;49:229.
- [11] Mooney PM, LeGoues FK, Tersoff J, Chu JO. *J Appl Phys* 1994;75:3968.
- [12] Koester SJ, Rim K, Chu JO, Mooney PM, Ott JA, Hargrove MA. *Appl Phys Lett* 2001;79:2148.
- [13] Gray JL, Hull R, Floro JA. *Appl Phys Lett* 2001;81:2445.
- [14] Lee H, Johnson JA, He MY, Speck JS, Petroff PM. *Appl Phys Lett* 2001;78:105.
- [15] Floro JA, Chason E, Freund LB, Twisten RD, Hwang RQ, Lucadamo GA. *Phys Rev* 1999;B59:1990.
- [16] Floro JA, Chason E, Sinclair MB, Freund LB, Lucadamo GA. *Appl Phys Lett* 1998;73:951.
- [17] Pan D, Xu J, Towe E, Xu Q, Hsu JW. *Appl Phys Lett* 1998;73:2164.
- [18] Shchukin VA, Ledentsov NN, Kop'ev PS, Bimberg D. *Phys Rev Lett* 1995;75:2968.
- [19] Leonard F, Desai RC. *Phys Rev* 1998;B58:8277.
- [20] Hirth JP, Lothe J. *Theory of dislocations*. Malabar (FL): Krieger, 1992.
- [21] Porter DA, Easterling KE. *Phase transformations in metals and alloys*. Berkshire, England: Van Nostrand Reinhold, 1981.
- [22] Gomez-Ramirez R, Pound GM. *Met Trans* 1973;4:1563.
- [23] Aaronson HI, Lee JK. In: Aaronson HI, editor. *Lectures on the theory of phase transformations*. New York: American Institute of Mining, Metallurgical and Petroleum Engineers; 1975.
- [24] Kalos MH, Whitlock PA. *Monte Carlo methods, volume I: basics*. New York: John Wiley and Sons, 1986.
- [25] Mahin KW, Hanson K, Morris Jr. JW. *Acta Metall* 1980;28:443.
- [26] Rickman JM, Tong WS, Barmak K. *Acta Mater* 1997;45:1153.
- [27] Metropolis N, Rosenbluth AW, Rosenbluth MN, Teller AH, Teller E. *J Chem Phys* 1953;21:1087.
- [28] Barmak K, Kim J, Shell S, Svedberg EB, Howard JK. *Appl Phys Lett* 2002;80:4268.
- [29] Sekimoto K. *Physica* 1986;135A:328.
- [30] Avrami M. *J Chem Phys* 1939;7:1103.
- [31] Cahn JW. *Acta Metall* 1956;4:449 More recent work in this area has focused on the "time-cone" method.
- [32] VanKampen NG. *Stochastic processes in physics and chemistry*. Amsterdam: North-Holland, 1992.
- [33] Tong WS, Rickman JM, Barmak K. *J Chem Phys* 2001;114:915.
- [34] Tomellini M, Fanfoni M, Volpe M. *Phys Rev* 2002;B6514:301.
- [35] Friedel J. *Dislocations*. New York: Pergamon Press, 1964.
- [36] Landau LD, Lifshitz EM. *Theory of elasticity*. New York: Pergamon Press, 1986.
- [37] Freund LB, Bower A, Ramirez JC. *Mater Res Soc Symp Proc* 1989;130:139.
- [38] Dundurs J. In: Mura T, editor. *Elastic interactions of dislocations with inhomogeneities in mathematical theory of dislocations*. New York: American Society of Mechanical Engineers; 1969.